

Specificity-Preserving Federated Learning for MR Image Reconstruction

Chun-Mei Feng^{1*}Yunlu Yan^{1*}Huazhu Fu²Yong Xu²Ling Shao³¹ Harbin Institute of Technology, Shenzhen² IHPC, A*STAR³ IIAI, UAE

Abstract

Federated learning (FL) can be used to improve data privacy and efficiency in magnetic resonance (MR) image reconstruction by enabling multiple institutions to collaborate without needing to aggregate local data. However, the domain shift caused by different MR imaging protocols can substantially degrade the performance of FL models. Recent FL techniques tend to solve this by enhancing the generalization of the global model, but they ignore the domain-specific features, which may contain important information about the device properties and be useful for local reconstruction. In this paper, we propose a specificity-preserving FL algorithm for MR image reconstruction (FedMRI). The core idea is to divide the MR reconstruction model into two parts: a globally shared encoder to obtain a generalized representation at the global level, and a client-specific decoder to preserve the domain-specific properties of each client, which is important for collaborative reconstruction when the clients have unique distribution. Moreover, to further boost the convergence of the globally shared encoder when a domain shift is present, a weighted contrastive regularization is introduced to directly correct any deviation between the client and server during optimization. Extensive experiments demonstrate that our FedMRI’s reconstructed results are the closest to the ground-truth for multi-institutional data, and that it outperforms state-of-the-art FL methods.¹

1. Introduction

Magnetic resonance (MR) imaging has become a mainstream diagnostic tool in radiology and medicine. However, its complex imaging process results in a longer acquisition time than other methods. To reduce the scanning time, several data-driven deep learning methods have been introduced, yielding outstanding improvements in MR image reconstruction [10, 36, 45, 46]. However, the superior results obtained by deep learning-based methods are dependent on

*The first two authors contribute equally to this work.

¹Our code is available at <https://github.com/chunmeifeng/FedMRI>.

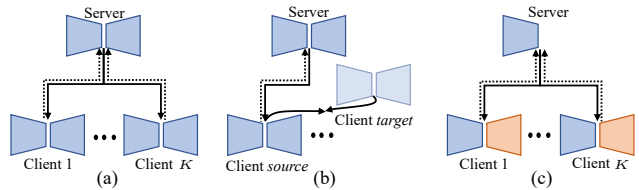


Figure 1. Classical FL algorithm for MR image reconstruction: (a) average all the local client models to obtain a general global model [24], or (b) repeatedly align the latent features between the source and target clients [9]. In contrast, we propose a *specificity-preserving* mechanism (c) to consider both “generalized shared information” as well as “client-specific properties”.

a large amount of diverse paired data, which is difficult to collect due to the patient privacy issues [31]. Recently, federated learning (FL) was proposed to provide a platform for different clients to learn collaboratively using local computing power, memory, and data without sharing any private local data [24, 42]. One of the standard and most widely used FL algorithms, FedAvg [24], collects local models of each client in each round of communication and distributes their average to each client for the next update (Fig. 1(a)). However, the different MR scanners and imaging protocols of different hospitals present heterogeneity [9], leading to a domain shift between clients [29]. Unfortunately, the generalization of models trained using FL may still be suboptimal under these conditions [9, 20]. Guo *et al.* tried to solve this problem by repeatedly aligning the latent features between the source and target clients (Fig. 1(b)), marking the first attempt to use FL in MR image reconstruction [9].

Although FL has been applied to MR image reconstruction [9], this cross-site approach requires sacrificing one client as the target site for alignment with other clients in each round. It is obvious that any client being used as a target site will result in privacy concerns, and the cross-site approach contradicts the purpose of FL, which is to prevent clients from communicating with each other through local data. Further, when the number of clients is large, the process becomes tedious because of the repeated training and frequent feature communication. More importantly, such a mechanism can only learn a general global model, ignoring the *client-specific properties*. Hence, we ask the following question: *Does the server really need to aver-*

age all the local client models during training? Ideally, it should consider not only 1) shared information but also 2) client-specific properties. Prior studies [39] in domain adaptation also suggest that the encoder is typically used to learn a shared representation to ensure that all inputs are equally suitable for any domain transformation. Therefore, we speculate that although FL algorithms have made some progress in MR image reconstruction [9], it is still possible to achieve higher-precision collaborative reconstruction when a domain shift is present by considering both 1) and 2).

With this insight, we propose a specificity-preserving FL algorithm for MR image reconstruction (FedMRI). Since each client has a specific domain distribution, we divide the MR image reconstruction model into two parts: a “globally shared encoder” to learn a *generalized representation*, and a “client-specific decoder” to enable each client to explore their *unique properties* under the presence of a domain shift (Fig. 1(c)). Further, to reduce the offset between client and server, we also introduce a weighted contrastive regularization term to *correct* the update direction for the global generalization. Specifically, it pulls the current client model (*anchor*) closer to the global model (*positive*) and pushes it away from its last update (*negative*). Our main **contributions** can be summarized as follows:

- We propose a *specificity-preserving* FL algorithm for MR image reconstruction, FedMRI, which learns a generalized globally shared encoder, while simultaneously providing a client-specific decoder for the local reconstruction. Our approach provides a more generalized representation and considers the local domain-specific information.
- We develop a *weighted contrastive regularization* for the globally shared part to relieve the domain drift of clients during training and boost the convergence.
- We demonstrate that significant performance improvements can be achieved with our specificity-preserving mechanism and weighted contrastive regularization, compared to averaging the local client models. Moreover, we also show that our partially shared model reduces the communication costs.

2. Related Works

MR Image Reconstruction. Reconstructing an MR image from undersampled k -space data is an ill-posed inverse problem. Traditional methods typically solve the problem using prior knowledge [23, 27, 35]. With the development of deep learning technology, CNN-based methods can directly learn the mapping from undersampled images to fully sampled data offline, which can greatly reduce the time of online reconstruction [40]. Benefiting from research in natural image synthesis, generative adversarial network

(GAN)-based methods using a generator and discriminator with a loss function have also been used to reconstruct MR images. Recently, transformers have also been applied in MR image reconstruction, providing more global information than CNNs [7, 12, 38]. However, all of these methods require the collection of large amounts of data. For medical data, this is not only labor-intensive but can also compromise patient privacy. We combine the data from different institutions for distributed joint training through FL, avoiding the dependence on large-scale data and the leakage of patients’ privacy.

Federated Learning. FL enables different clients to collaborate in training shared models, while maintaining data privacy [15, 16, 24]. However, the classical FL algorithm, FedAvg, does not address the domain shift caused by the statistical heterogeneity across various clients. More recent studies solve the feature shift and domain generalization problem caused by different data distributions through batch normalization and episodic learning in a continuous frequency space [20, 22]. In the classification task, efforts have also been made to keep parts of the network local to improve the accuracy [1, 4, 21]. For example, to provide a global head, Liang *et al.* send the classification head to the server for averaging [21]. However, the data typically shares a global representation in the body, and the statistical heterogeneity between clients or tasks is concentrated in the head. Their model must therefore first learn a generalized representation, and then use the local head to train the client-specific data on the client.

FL has also been applied to some medical tasks to protect patient privacy [5, 18, 19, 32, 32]. For example, in MR image reconstruction, Guo *et al.* repeatedly aligned the data distribution between the source and target client to reduce the data heterogeneity between them [9]. However, this frequent communication between clients may reduce the communication efficiency and cause privacy leakage. Therefore, the effectiveness of the privacy protection mechanism of MR image reconstruction based on FL needs to be further studied. We introduce a *specificity-preserving* FL mechanism that considers both the shared information and unique properties of clients. Though a few concurrent works also consider using a personalized layer for classification tasks, their premise is markedly different [1, 21]. First, they often assume that only the last layer can be considered as the personalized part. Second, they reduce the domain shift problems by learning global heads, which is opposite to our approach (see §4 for more details). Third, no one has ever attempted to progressively correct the update direction during training to reduce offsets and speed up convergence (§3.2).

Shared Representation Learning. In domain adaptation, the encoder is often used to learn a shared representation to ensure that all inputs are equally suitable for any domain transformation [3, 11, 30, 39]. This has also been applied

to other fields [11, 26, 33]. For example, for classification, Sanchez *et al.* [33] used a low-dimensional shared representation to capture a generalized representation between images. Nam *et al.* [26] used shared layers to learn the generalized features of different domains, while employing the domain-specific layers of different branches to learn domain-specific properties for visual tracking. This is similar to our approach for solving the domain shift problem of multi-institutional MR image reconstruction with a universal feature representation. Differently, however, we focus on privacy-protected distribution computing, where no data is communicated between clients.

3. Proposed Method

3.1. FL for MR Image Reconstruction

MR image reconstruction aims to directly learn a mapping from undersampled to fully-sampled data in the image domain, where the undersampled data is obtained by accelerating the k -space data acquisition in the frequency domain [8, 9, 28, 37]. An image can then be obtained by inverse multi-dimensional Fourier transform \mathcal{F}^{-1} of the measured k -space points. Let $\mathbf{k} \in \mathbb{C}^M$ represent the observed k -space measurement, and $\mathbf{x} \in \mathbb{C}^M$ represent the undersampled image. The relationship between them can be formulated as follows:

$$\mathbf{x} = \mathcal{F}^{-1}(\mathbf{k} + \epsilon) = \mathcal{F}^{-1}(M \odot \mathcal{F}(\mathbf{y}) + \epsilon), \quad (1)$$

where ϵ is the measurement noise, \odot is an element-wise multiplication operation, M is the binary mask operator to select a subset of the k -space points, and \mathbf{y} is the fully sampled image. Reconstructing \mathbf{x} from the limited sampled data is an ill-posed inverse problem and we can obtain a more feasible solution by CNNs:

$$\mathcal{L}_{rec} = \frac{1}{N} \sum_{n=1}^N \|f(\mathbf{x}; \mathbf{w}) - \mathbf{y}\|_1, \quad (2)$$

where $f(\mathbf{x})$ is the network parameterized by \mathbf{w} , and N is the number of training samples.

Eq. (2) trains all of the hospital data together, resulting in the privacy of patients being leaked. If we train the data of each hospital in a distributed way using an FL framework, patient privacy can be protected. Suppose there are K hospitals/clients. The local datasets of each client can be denoted as $\mathcal{D}^1, \mathcal{D}^2, \dots, \mathcal{D}^K$, which contain pairs of undersampled and fully-sampled images. For each client, we train a local model by minimizing the following loss:

$$\mathcal{L}_{rec} = \frac{1}{K} \sum_{k=1}^K \|G^k(\mathbf{x}; \Theta_{G^k}) - \mathbf{y}\|_1, \quad (3)$$

where $G^k(\mathbf{x}; \Theta_{G^k})$ corresponds to the reconstructed image $\hat{\mathbf{y}}$, and G^k is the local model of client k parameterized by

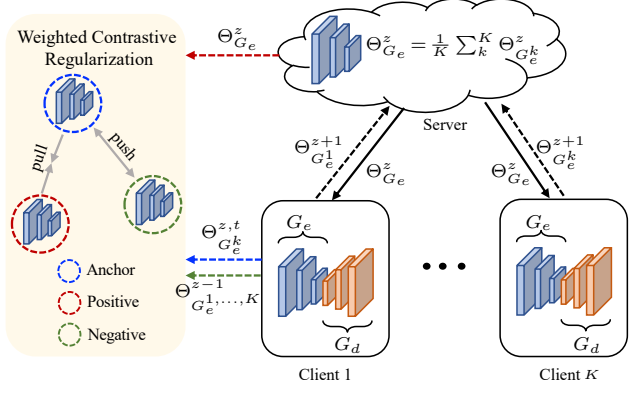


Figure 2. **Overview of the FedMRI framework.** Instead of averaging all the local client models, a “globally shared encoder”  is used to obtain a generalized representation, and a “client-specific decoder”  is used to explore unique domain-specific information. We apply the weighted contrastive regularization to better pull (\leftrightarrow) the positive pairs (, ) together and push (\leftrightarrow) the negative () ones towards the anchor.

Θ_{G^k} . In each round $z = 1, \dots, Z$, the local model parameter of client k at local epoch t is updated by the following optimization:

$$\Theta_{G^k}^{z,t+1} = \Theta_{G^k}^{z,t} - \eta_k \nabla \mathcal{L}(\mathbf{x}^k; \Theta_{G^k}^{z,t}), \quad (4)$$

where η_k is the learning rate of client k , and t is the number of local updates. All participating clients send their updated weights to the central server after completing each round of training locally. The central server then provides a global model by averaging all local parameters. It can be defined as follows:

$$\Theta_G^z = \frac{1}{K} \sum_{k=1}^K \Theta_{G^k}^z, \quad (5)$$

where $\Theta_{G^k}^z$ represents the model parameter of client k in the current global training round z . After Z rounds of communication, the final global model parameterized by Θ_G^Z can be trained with multi-domain information without directly sharing the private data of each client.

3.2. Architecture of FedMRI

Our network architecture uses U-Net as the base framework for clients, where the encoder extracts latent features and the decoder generates images. As shown in Fig. 2, we share the encoder with the central server to extract a global generalized representation, and the decoder is kept local to explore the unique local depth information. To alleviate the bias of local updates, a weighted contrastive regularization term is used to constrain the updating direction of the gradient during the iteration process.

FedMRI aims to find the optimal unique information for each client, while the server and client learn the global generalized representation together (see Fig. 2). To this end,

each round of FedMRI communication alternates between client updates and server updates. We consider dividing the reconstruction model G^k into G_e^k and G_d^k for sharing global and finding unique deep properties, respectively. Thus, the objective of Eq. (3) can be rewritten as:

$$\mathcal{L}_{rec} = \frac{1}{K} \sum_{k=1}^K \| (G_e(\mathbf{x}) \circ G_d^k(\mathbf{x})) - \mathbf{y} \|_1, \quad (6)$$

where G_e and G_d^k represent the globally shared encoder and a client-specific decoder, respectively. Note that the global representation G_e is jointly learnt by the server and client, while unique domain-specific information is explored by each client. The alternate update rules between the client and server in each round of communication are as follows.

Client Update Step: The client updates the local gradient based on the global representation currently transmitted by the server to find the optimal unique local properties:

$$\Theta_{G_d^k}^{z,t+1} = \Theta_{G_d^k}^{z,t} - \eta_k \nabla \mathcal{L}_{cl} \left(\Theta_{G_e}^z \cup \Theta_{G_d^k}^{z,t}; \mathbf{x}^k \right), \quad (7)$$

where $\Theta_{G_e}^z \cup \Theta_{G_d^k}^{z,t} = \Theta_{G^k}^{z,t}$. The advantage of this update rule is that the number of local updates can be controlled to find the optimal client-specific decoder based on the local data (see section §4.2).

Server Update Step: After the local update epoch is complete, the client participates in the global gradient update in the server as follows:

$$\Theta_{G_e^k}^{z+1} = \Theta_{G_e^k}^z - \eta_k \nabla \mathcal{L}_{se} \left(\Theta_{G_e^k}^z \cup \Theta_{G_d^k}^{z,T}; \mathbf{x}^k \right). \quad (8)$$

Then, we send $\Theta_{G_e^k}^{z+1}$ to the server and average them to compute the next global representation $\Theta_{G_e}^{z+1}$.

Weighted Contrastive Regularization: Although we have shared the weight $\Theta_{G_e}^z$ to the server to find the generalized representation among the clients, there is always an offset between $\Theta_{G_e}^z$ and $\Theta_{G_e^k}^{z+1}$ during iterative optimization, mainly caused by the domain shift during local optimization. To further correct the local updates and provide the model with global recognition ability, we introduce weighted contrastive regularization between the local and global encoders to force G_e^k to learn a stronger generalized representation. Instead of finding positive and negative pairs from data, we directly regularize the update direction on the network parameters, which is different from traditional contrastive learning. This enables the gradient updates to be corrected more directly, without relying on a large batch size [43]. Our experimental results also support this, as shown in Table 3.

Suppose the client k performs a local update, it first receives global parameters $\Theta_{G_e}^z$ from the server and then performs a local iterative update based on these. However, the

Algorithm 1: FedMRI

Input: Datasets from K clients: $\mathcal{D}^1, \mathcal{D}^2, \dots, \mathcal{D}^K$; number of local updates T ; number of communication rounds Z ; hyperparameter μ ; learning rate for client k : η_k ;

Output: The final global model parameter Θ_{G_e} ;

```

1 for  $z = 1, 2, \dots, Z$  do
2   for  $k = 1, 2, \dots, K$  do
3     receive the global model from the server;
4     for  $t = 1, 2, \dots, T$  do
5        $\Theta_{G_d^k}^{z,t+1} \leftarrow \Theta_{G_d^k}^{z,t} - \eta_k \nabla \mathcal{L}_{cl};$ 
6     end
7     client locally update the representation and
      sends it to the server:
8      $\Theta_{G_e^k}^{z+1} \leftarrow \Theta_{G_e^k}^z - \eta_k \nabla \mathcal{L}_{se};$ 
9      $\mathcal{L}_{con} \leftarrow \text{ContrastiveLoss}$ 
10     $\left( \Theta_{G_e^k}^{z,t}; \{\Theta_{G_e^i}^{z-1}, i \in K\}; \Theta_{G_e}^z; \mathbf{x} \right);$ 
11     $\mathcal{L}_{rec} \leftarrow \text{SupervisedLoss}$ 
12     $\left( \Theta_{G_e}^z \cup \Theta_{G_d^k}^{z,T}; (\mathbf{x}, \mathbf{y}) \right);$ 
13     $\mathcal{L} = \mathcal{L}_{rec} + \mu \mathcal{L}_{con};$ 
14  end
15 end

```

average to get the new representation.

15 **end**

global parameters from the server always have less bias than the local parameters. Following [41], we use the \mathcal{L}_1 distance to measure the difference between the two models. Thus, our weighted contrastive regularization loss can be defined as:

$$\mathcal{L}_{con} = \frac{\left\| \Theta_{G_e^k}^{z,t} - \Theta_{G_e}^z \right\|_1}{\sum_{i=1}^K \left\| \Theta_{G_e^i}^{z-1} - \Theta_{G_e^k}^{z,t} \right\|_1}. \quad (9)$$

Combined with the supervised reconstruction loss, the overall loss of our model can be expressed as:

$$\mathcal{L} = \mathcal{L}_{rec} \left(\Theta_{G_e}^z \cup \Theta_{G_d^k}^{z,T}; (\mathbf{x}, \mathbf{y}) \right) + \mu \mathcal{L}_{con} \left(\Theta_{G_e^k}^{z,t}; \{\Theta_{G_e^i}^{z-1}, i \in K\}; \Theta_{G_e}^z; \mathbf{x} \right), \quad (10)$$

where μ is a hyperparameter that controls the weight of the weighted contrastive regularization term.

The detailed procedure is outlined in Algorithm 1. In each round of communication, the server sends the global model to each client. Each client then performs local gradient updating according to the global representation currently transmitted by the server to acquire its optimal unique information, as shown in Eq. (7). Then, the client participates in the server update according to Eq. (8) and corrects the local gradient updates.

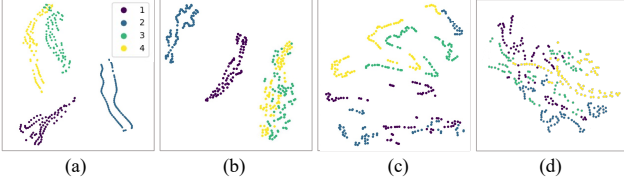


Figure 3. T-SNE visualizations of latent features from four datasets: • fastMRI [44], • BraTS [25], • SMS [6], and • uMR [6]. (a) Distribution of SingleSet, where each client is trained with their local data without FL; (b) Distribution of FedAvg; (c) Distribution of our FedMRI without \mathcal{L}_{con} ; (d) Distribution of our entire FedMRI algorithm.

3.3. Comparison with Standard FL

Our main idea is in line with the domain adaption techniques, where a shared encoder learns a domain-invariant representation to ensure that all inputs are equally suitable for any domain transformation [11], while the decoder maintains the domain-special representation. Similarly, in FL for MR image reconstruction, an ideal model should consider both the shared information and client-specific properties. Naturally, we can send the encoder of each client back to the server to learn a generalized representation, while the decoder is kept in local clients to explore the unique client-specific properties.

To further verify our idea, we visualize the T-SNE distributions of latent features in Fig. 3, where (a-d) show the distributions of SingleSet, FedAvg [24], FedMRI without \mathcal{L}_{con} , and our entire FedMRI algorithm, respectively. In SingleSet, each client is trained to use their local data without FL. The distribution of points in (a) is clearly differentiated because each dataset has its own biases, while the data in (b), (c) and (d) overlap to varying degrees, as these models benefit from the joint training mechanism of FL. However, on the datasets with large differences in distribution, *e.g.*, fastMRI and Brats, FedAvg [24] nearly fails (see Fig. 3 (b)). Notably, even without \mathcal{L}_{con} , our method still aligns the latent space distribution across the four different datasets, which demonstrates that sharing a global encoder and keeping a client-specific decoder can effectively reduce the domain shift problem (see Fig. 3 (c)). Fig. 3 (d) shows a fully mixed distribution for the latent features of the different clients. This can be attributed to the weighted contrastive regularization, which enables our FedMRI algorithm to effectively correct deviations between the client and server during optimization (see Fig. 3 (d)).

4. Experiments

In this section, we present the datasets, implementations, and experiments in detail. Our studies 1) a comparison in reconstruction accuracy with the current state of the arts under different Scenarios (Scenario 1 is a multi-institutional collaboration with local data, and Scenario

2 is a multi-institutional collaboration with a higher domain shift); 2) an evaluation of communication efficiency and the influence of local updates on the global representation; and 3) an ablation study of the key components in our method.

4.1. Experimental Setup

Implementation Details. Following [9], a U-Net style architecture is adopted for the reconstruction networks. We train our method using Pytorch with eight NVIDIA Tesla V100 GPUs and 32GB of memory per card. The batch size and initial learning rate are set to 8 and 1×10^{-4} , respectively. The models are trained using an RMSProp optimizer, and 50 communication rounds with 10 local epochs each. The hyperparameter μ is empirically set to 100. We tested and found that our method converges after 50 communication rounds, and achieves the best results when $\mu=100$ (see Fig. 5 and Fig. 6).

Baselines. We compare against various state-of-the-art models to demonstrate the effectiveness of our method. These include: (1) SingleSet, in which each client is trained using their local data without FL; (2) FedAvg [24], which trains a global model by averaging the parameters from all participating clients; (3) FL-MRCM [9], which removes the domain shift during multi-institutional MR imaging collaboration by aligning the latent features between the source and target clients; (4) GD-GD [1], which explores a personalized layer after the base part; (5) LG-FedAvg [21], which attempts to learn the local heads and a global network body, as an opposite to our approach; (6) FedBN [20], which alleviates the domain shift by applying local batch normalization; and (7) FedProx [17], which adds a proximal term to the objective function of the local model. For fair comparison, we adopt U-Net as the reconstruction network of each client for all the baselines.

Datasets. We employ four different datasets with different distributions as the clients in the FL setting. Each dataset is divided with a ratio of 7:3 for local train/test.

- **fastMRI** [44]: 2,134 brain subjects with 16 T1 and 16 T2 weighted slices each are used in our experiments.
- **BraTS** [25]: 385 brain subjects with 80 T1 weighted and 80 T2 weighted slices each are adopted.
- **SMS** [6]: 155 subjects are collected by a 3T Siemens Magnetom Skyra system, with 20 T1 and 20 T2 weighted slices each.
- **uMR** [6]: 50 subjects are collected by a United Imaging Healthcare uMR 790 scanner, with 20 T1 weighted and 20 T2 weighted slices each.

4.2. Experimental Results

Accuracy Comparison. To verify the effectiveness of our FL approach, FedMRI, in multi-institutional collaboration, we compare it with various state-of-the-art FL algorithms.

Table 1. **Quantitative comparison** of state-of-the-art FL methods under Scenario 1, with *1D uniform* sampling and $3\times$ acceleration. See §4.2 for more details.

Method	fastMRI [44]		BraTS [25]		SMS [6]		uMR [6]		Average	
	PSNR↑	SSIM↑								
SingleSet	36.88	0.936	32.74	0.911	25.20	0.758	23.50	0.683	29.58	0.822
FedAvg [24]	36.56	0.933	32.90	0.908	25.25	0.722	21.09	0.646	28.95	0.802
FedBN [20]	29.40	0.853	28.85	0.713	29.44	0.855	30.73	0.879	29.61	0.825
FL-MRCM [9]	30.05	0.736	30.50	0.780	30.66	0.859	29.38	0.888	30.04	0.816
FedProx [17]	36.13	0.902	31.16	0.813	29.02	0.887	29.54	0.889	31.46	0.873
LG-FedAvg [21]	37.04	0.940	32.52	0.899	30.00	0.834	28.31	0.861	31.97	0.884
GD-GD [1]	38.05	0.959	32.89	0.939	34.79	0.939	35.90	0.950	35.41	0.947
FedMRI	39.51	0.970	33.93	0.951	35.10	0.944	36.49	0.954	36.26	0.955

Table 2. **Quantitative comparison** of state-of-the-art FL methods under Scenario 2, with different undersampling patterns and various acceleration rates (*e.g.*, *1D uniform* $3\times$, *1D Cartesian* $5\times$, *2D radial* $4\times$, and *2D random* $6\times$). See §4.2 for more details.

Method	fastMRI [44]		BraTS [25]		SMS [6]		uMR [6]		Average	
	<i>1D uniform</i> $3\times$ PSNR↑	SSIM↑	<i>1D Cartesian</i> $5\times$ PSNR↑	SSIM↑	<i>2D radial</i> $4\times$ PSNR↑	SSIM↑	<i>2D random</i> $6\times$ PSNR↑	SSIM↑	PSNR↑	SSIM↑
SingleSet	35.26	0.925	29.66	0.869	24.49	0.771	24.25	0.661	28.41	0.806
FedAvg [24]	35.53	0.920	29.82	0.872	23.95	0.734	24.19	0.675	28.37	0.800
FedBN [20]	31.28	0.787	29.95	0.885	26.87	0.817	26.73	0.790	28.71	0.820
FL-MRCM [9]	30.16	0.772	28.04	0.760	28.48	0.857	29.33	0.864	29.00	0.813
FedProx [17]	35.29	0.920	29.82	0.881	28.80	0.895	29.28	0.902	30.79	0.900
LG-FedAvg [21]	36.75	0.952	29.91	0.873	32.56	0.923	33.35	0.923	33.14	0.918
GD-GD [1]	38.00	0.959	30.07	0.902	37.02	0.970	37.28	0.959	35.59	0.948
FedMRI	39.74	0.971	31.18	0.919	38.17	0.970	37.74	0.963	36.71	0.956

For fair comparison, we retrain them on MR data and report their optimal results. For FedProx, we tune its hyperparameter μ within $\{0.001, 0.01, 0.1, 1\}$ and report the best result at 0.01. All the compared methods are trained over 70 communication rounds with 10 local epochs each, because they all converge at round 70 (see section §4.2). Table 1 shows the reconstruction results of all methods under Scenario 1, which employs *1D uniform* sampling with $3\times$ acceleration. Our FedMRI is superior to all the other methods in both PSNR and SSIM. In particular, on small datasets, such as **SMS** and **uMR**, our method improves the PSNR results of FedAvg from 25.25 dB and 21.09 dB to **35.10** dB and **36.49** dB, respectively. This demonstrates that FedMRI can effectively remove the domain shift in the non-iid datasets. The distributed training on data from multiple institutions without compromising privacy can solve the dependence of traditional deep learning on the collection of big data.

Robustness to a Higher Domain-Shift Setting. To further evaluate the robustness of our method, we record the results of each client under different sampling patterns and accelerations in Table 2. Considering that various hospital scanners use different scanners, we employ different undersampling patterns, *e.g.*, *1D uniform* $3\times$, *1D Cartesian* $5\times$, *2D radial* $4\times$, and *2D random* $6\times$, to set up Scenario 2. As expected, our method achieves better results under a higher domain shift. In contrast, the FedAvg and MRI multi-institutional collaboration method, FL-MRCM,

performs worse under this scenario. Compared with other methods, FedMRI is most robust because it can balance the learning of local and global representations, ensuring that the client learns unique client-specific properties.

In addition, it is worth noting that our method also outperforms the personalized FL methods, *e.g.*, GD-GD [1] and LG-FedAvg [21], in both Scenario 1 and 2. Since GD-GD only keeps the last layer as the personalized layer after the base part, which damages the strong unique local properties, there is almost no improvement in the higher domain shift setting. LG-FedAvg shares a global decoder/network body and learns a local encoder/head, which is opposite to our approach, resulting in a poor generalized representation. The results support our previous suggestion that an ideal personalized mechanism must train shared information before the client-specific property. Therefore, the most effective personalized mechanism for MR image reconstruction is to use latent features to obtain a generalized representation first and then preserve the unique domain-specific properties in each client.

To qualitatively evaluate our method, we visualize the reconstructed images and corresponding error maps of all the compared methods for Scenario 2 in Fig. 4. The less texture in the error map, the better the reconstruction. As can be seen from the figure, our method reconstructs the best-quality images and significantly reduces errors. The reconstructed images and corresponding error maps for

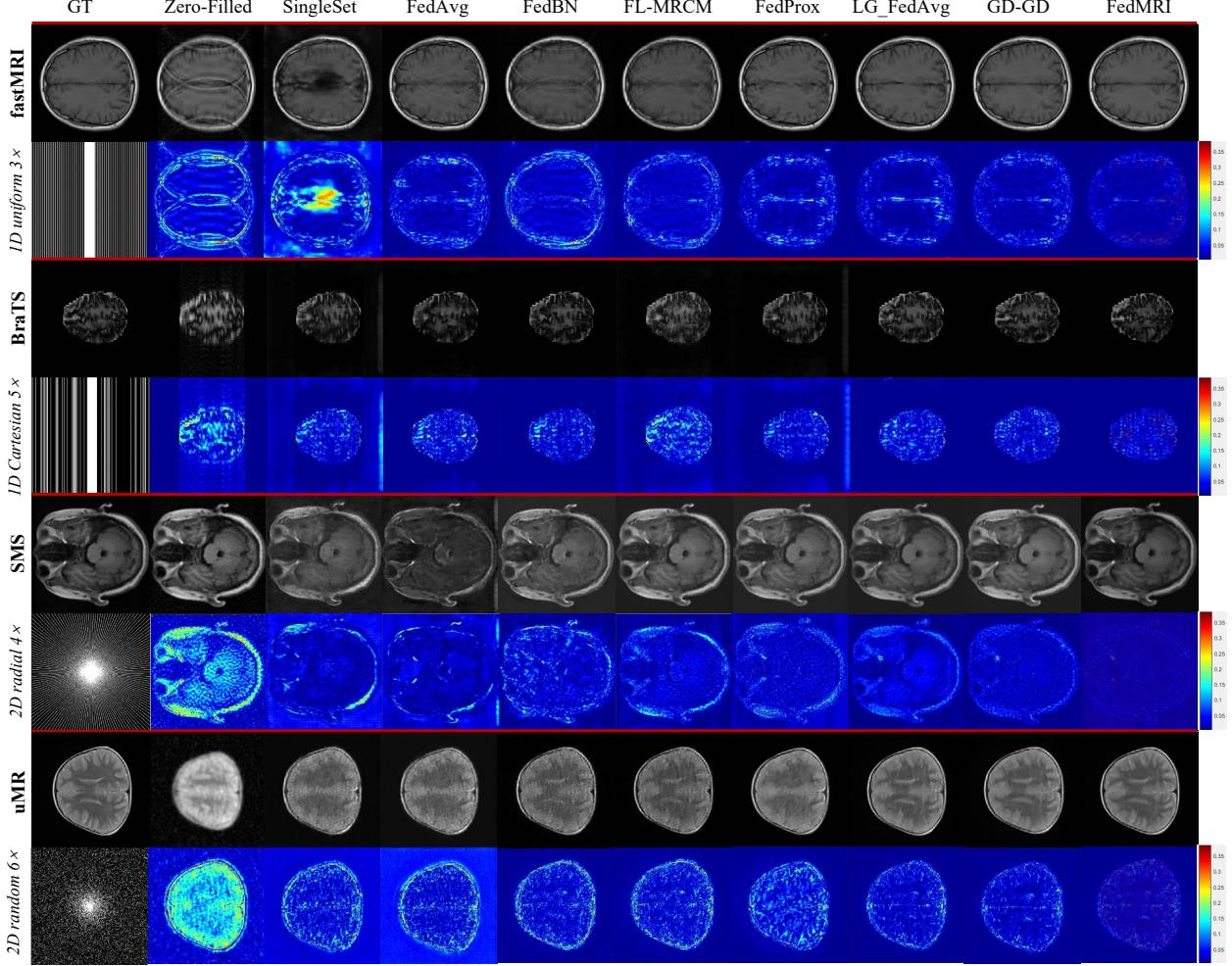


Figure 4. **Qualitative comparison** of different methods in terms of reconstruction quality and error maps under Scenario 2.

Table 3. **Ablation study of the key components** in our method, where G_e^k and G_d^k are the shared part of the FL model, and \mathcal{L}_{con}^f and \mathcal{L}_{con}^w represent the contrastive regularization based on features and weights, respectively. See §4.3 for more details.

Methods	G_e^k	G_d^k	fastMRI [44]		BraTS [25]		SMS [6]		uMR [6]		Average	
			PSNR	SSIM	PSNR	SSIM	PSNR	SSIM	PSNR	SSIM	PSNR	SSIM
\mathcal{M}_1	✓	✓	✗	✗	35.53	0.920	29.82	0.872	23.95	0.734	24.19	0.675
\mathcal{M}_2	✓	✗	✗	✗	38.42	0.962	30.24	0.915	37.36	0.968	37.44	0.959
\mathcal{M}_3	✓	✗	✓	✗	36.29	0.938	29.07	0.805	34.84	0.876	34.08	0.841
Ours	✓	✗	✗	✓	39.74	0.971	31.18	0.919	38.17	0.970	37.74	0.963
											36.71	0.956

Scenario 1 can be found in the *Appendix*.

Communication Efficiency. In Fig. 5, we compare the accuracy of all methods in each round to demonstrate the superior communication efficiency of our method, where FedMRI † represents our model without weighted contrastive regularization. Note that the local epochs are set to 10 for all the compared methods. As can be seen from the figure, FedMRI † achieves stability in the fifth round. The other methods improve most in the first five rounds, but do

not achieve stability until after more than 50 rounds. With the help of weighted contrastive regularization, our FedMRI converges much faster than FedMRI † because it corrects the deviation between the client and server during optimization. As we have mentioned that weighted contrastive regularization can boost the convergence, the results in this figure confirm our previous conjecture. This means that our method has the highest communication efficiency, which is one of the important issues in FL [13].

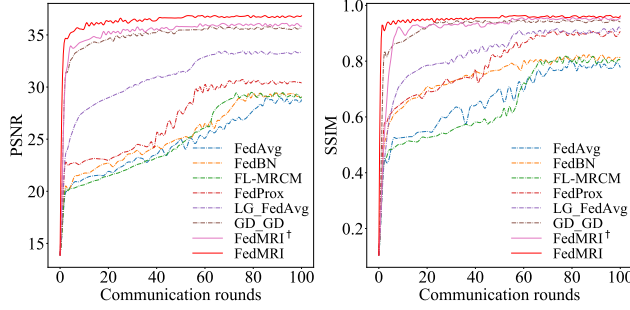


Figure 5. **Analysis of communication efficiency** in terms of PSNR and SSIM.

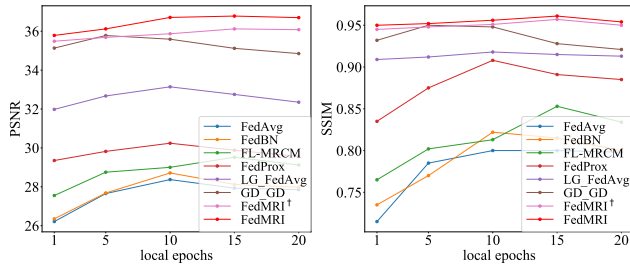


Figure 6. **Analysis of different numbers of local epochs** in terms of PSNR and SSIM.

Benefit of Local Updates. The domain shift problem between clients causes the server to deviate from the global optimal solution when averaging. As mentioned in §1, considering both the shared generalized representation and client-specific properties helps mitigate this problem. In Fig. 6, we explore whether more local epochs can enhance the generalized representation to address the bias from the global optimal solution. From this figure, we observe that increasing the number of local epochs improves both FedMRI[†] and FedMRI significantly compared to other FL methods. Further, when the number of local epochs is too large, the reconstruction accuracy of other methods decreases. In contrast, for our method, more local epochs can alleviate the divergence from the global optimal solution without damaging local computations.

4.3. Ablation Study

In this section, we first investigate the crucial components in our method, *e.g.*, the shared part of the local client (G_e^k and G_d^k), and weighted contrastive regularization. For comparison, we build two baselines, \mathcal{M}_1 and \mathcal{M}_2 , which represent our model without the partially shared network and weighted contrastive regularization respectively. As shown in Table 3, we conduct tests under Scenario 2. \mathcal{M}_1 performs the worst, indicating that partially sharing the representation makes it possible to train on different clients with different domains. Since the weighted contrastive regularization term corrects the offsets of local client updates,

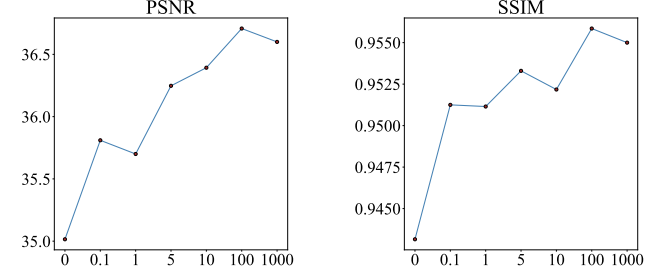


Figure 7. **Analysis of weighted contrastive regularization** hyperparameter μ in terms of PSNR and SSIM.

the generalized representation learned by \mathcal{M}_2 is not optimal when this term is lost. In addition, we also investigate the effect of using traditional contrastive learning (see \mathcal{M}_3), which adopts the positive and negative feature pairs, as mentioned in [14]. As can be seen, \mathcal{M}_3 is far inferior to directly imposing contrastive regularization on the parameters, which can directly correct the gradient updates and does not depend on a large batch size. Our FedMRI obtains the best results thanks to its two crucial parts, proving its strong ability in removing the domain shift.

Finally, we investigate the influence of the weighted contrastive regularization hyperparameter μ in our method. Fig. 7 shows the PSNR and SSIM values from $\{0, 1, 10, 100, 1000\}$. From the figure, we observe that the reconstruction accuracy increases with increasing μ . Setting $\mu = 100$ yields the best results, with the weighted contrastive regularization leading to substantial performance gains in PSNR (*i.e.*, 35.87 dB \rightarrow **36.71** dB). When μ is greater than 100, the performance degrades due to an overly large weight, which affects the unique information learning of the local client.

5. Conclusion

In this work, we focus on the domain shift problem in MR image reconstruction using multi-institutional data in a privacy-protected manner. To this end, we propose a specificity-preserving federated learning for MR image reconstruction (FedMRI). By employing a globally shared encoder to learn a generalized representation and a client-specific decoder to explore unique domain-specific properties, our proposed FedMRI can obtain the most effective global representation and simultaneously preserve the domain characteristics of client-side. Further, the weighted contrastive regularization term corrects the bias of local clients during each iteration, forcing the shared encoder to learn the global representation. Extensive experiments on multiple datasets from different domains demonstrate that our method can achieve MR image reconstruction joint multi-institutional client. Given the need for privacy protection in medical data, we expect further innovations in MR image reconstruction by federated learning.

References

[1] Manoj Ghuhan Arivazhagan, Vinay Aggarwal, Aaditya Kumar Singh, and Sunav Choudhary. Federated learning with personalization layers. *arXiv preprint arXiv:1912.00818*, 2019. 2, 5, 6, 11

[2] Ting Chen, Simon Kornblith, Mohammad Norouzi, and Geoffrey Hinton. A simple framework for contrastive learning of visual representations. In *International conference on machine learning*, pages 1597–1607. PMLR, 2020. 11

[3] Safa Cicek and Stefano Soatto. Unsupervised domain adaptation via regularized conditional alignment. In *Proceedings of the IEEE/CVF International Conference on Computer Vision*, pages 1416–1425, 2019. 2

[4] Liam Collins, Hamed Hassani, Aryan Mokhtari, and Sanjay Shakkottai. Exploiting shared representations for personalized federated learning. *arXiv preprint arXiv:2102.07078*, 2021. 2

[5] Ines Feki, Sourour Ammar, Yousri Kessentini, and Khan Muhammad. Federated learning for covid-19 screening from chest x-ray images. *Applied Soft Computing*, 106:107330, 2021. 2

[6] Chun-Bei Feng, Huazhu Fu, Shuhao Yuan, and Yong Xu. Multi-contrast mri super-resolution via a multi-stage integration network. In *International Conference on Medical Image Computing and Computer Assisted Intervention (MICCAI)*, 2021. 5, 6, 7, 12

[7] Chun-Bei Feng, Yunlu Yan, Geng Chen, Huazhu Fu, Yong Xu, and Ling Shao. Accelerated multi-modal mr imaging with transformers. *arXiv e-prints*, pages arXiv–2106, 2021. 2

[8] Chun-Bei Feng, Zhanyuan Yang, Geng Chen, Yong Xu, and Ling Shao. Dual-octave convolution for accelerated parallel mr image reconstruction. *arXiv preprint arXiv:2104.05345*, 2021. 3

[9] Pengfei Guo, Puyang Wang, Jinyuan Zhou, Shanshan Jiang, and Vishal M Patel. Multi-institutional collaborations for improving deep learning-based magnetic resonance image reconstruction using federated learning. In *Proceedings of the IEEE/CVF Conference on Computer Vision and Pattern Recognition*, pages 2423–2432, 2021. 1, 2, 3, 5, 6, 11

[10] Kerstin Hammernik, Teresa Klatzer, Erich Kobler, Michael P Recht, Daniel K Sodickson, Thomas Pock, and Florian Knoll. Learning a variational network for reconstruction of accelerated mri data. *Magnetic resonance in medicine*, 79(6):3055–3071, 2018. 1

[11] Lanqing Hu, Meina Kan, Shiguang Shan, and Xilin Chen. Duplex generative adversarial network for unsupervised domain adaptation. In *Proceedings of the IEEE Conference on Computer Vision and Pattern Recognition*, pages 1498–1507, 2018. 2, 3, 5

[12] Salman Khan, Muzammal Naseer, Munawar Hayat, Syed Waqas Zamir, Fahad Shahbaz Khan, and Mubarak Shah. Transformers in vision: A survey. *arXiv preprint arXiv:2101.01169*, 2021. 2

[13] Jakub Konečný, H Brendan McMahan, Felix X Yu, Peter Richtárik, Ananda Theertha Suresh, and Dave Bacon. Federated learning: Strategies for improving communication efficiency. *arXiv preprint arXiv:1610.05492*, 2016. 7

[14] Qinbin Li, Bingsheng He, and Dawn Song. Model-contrastive federated learning. In *Proceedings of the IEEE/CVF Conference on Computer Vision and Pattern Recognition*, pages 10713–10722, 2021. 8

[15] Qinbin Li, Zeyi Wen, Zhaomin Wu, Sixu Hu, Naibo Wang, Yuan Li, Xu Liu, and Bingsheng He. A survey on federated learning systems: vision, hype and reality for data privacy and protection. *arXiv preprint arXiv:1907.09693*, 2019. 2

[16] Tian Li, Anit Kumar Sahu, Ameet Talwalkar, and Virginia Smith. Federated learning: Challenges, methods, and future directions. *IEEE Signal Processing Magazine*, 37(3):50–60, 2020. 2

[17] Tian Li, Anit Kumar Sahu, Manzil Zaheer, Maziar Sanjabi, Ameet Talwalkar, and Virginia Smith. Federated optimization in heterogeneous networks. *arXiv preprint arXiv:1812.06127*, 2018. 5, 6, 11

[18] Wenqi Li, Fausto Milletari, Daguang Xu, Nicola Rieke, Jonny Hancox, Wentao Zhu, Maximilian Baust, Yan Cheng, Sébastien Ourselin, M Jorge Cardoso, et al. Privacy-preserving federated brain tumour segmentation. In *International workshop on machine learning in medical imaging*, pages 133–141. Springer, 2019. 2

[19] Xiaoxiao Li, Yufeng Gu, Nicha Dvornek, Lawrence H Staib, Pamela Ventola, and James S Duncan. Multi-site fmri analysis using privacy-preserving federated learning and domain adaptation: Abide results. *Medical Image Analysis*, 65:101765, 2020. 2

[20] Xiaoxiao Li, Meirui Jiang, Xiaofei Zhang, Michael Kamp, and Qi Dou. Fedbn: Federated learning on non-iid features via local batch normalization. *arXiv preprint arXiv:2102.07623*, 2021. 1, 2, 5, 6, 11

[21] Paul Pu Liang, Terrance Liu, Liu Ziyin, Nicholas B Allen, Randy P Auerbach, David Brent, Ruslan Salakhutdinov, and Louis-Philippe Morency. Think locally, act globally: Federated learning with local and global representations. *arXiv preprint arXiv:2001.01523*, 2020. 2, 5, 6, 11

[22] Quande Liu, Cheng Chen, Jing Qin, Qi Dou, and Pheng-Ann Heng. Feddg: Federated domain generalization on medical image segmentation via episodic learning in continuous frequency space. In *Proceedings of the IEEE/CVF Conference on Computer Vision and Pattern Recognition*, pages 1013–1023, 2021. 2

[23] Angshul Majumdar, Rabab K Ward, and Tyseer Aboulnasr. Non-convex algorithm for sparse and low-rank recovery: Application to dynamic mri reconstruction. *Magnetic resonance imaging*, 31(3):448–455, 2013. 2

[24] Brendan McMahan, Eider Moore, Daniel Ramage, Seth Hampson, and Blaise Aguera y Arcas. Communication-efficient learning of deep networks from decentralized data. In *Artificial intelligence and statistics*, pages 1273–1282. PMLR, 2017. 1, 2, 5, 6, 11

[25] Bjoern H Menze, Andras Jakab, Stefan Bauer, Jayashree Kalpathy-Cramer, Keyvan Farahani, Justin Kirby, Yuliya Burren, Nicole Porz, Johannes Slotboom, Roland Wiest, et al. The multimodal brain tumor image segmentation benchmark (brats). *IEEE transactions on medical imaging*, 34(10):1993–2024, 2014. 5, 6, 7, 12

[26] Hyeonseob Nam and Bohyung Han. Learning multi-domain convolutional neural networks for visual tracking. In *Pro-*

ceedings of the IEEE conference on computer vision and pattern recognition, pages 4293–4302, 2016. 3

[27] Ricardo Otazo, Emmanuel Candes, and Daniel K Sodickson. Low-rank plus sparse matrix decomposition for accelerated dynamic mri with separation of background and dynamic components. *Magnetic resonance in medicine*, 73(3):1125–1136, 2015. 2

[28] Chen Qin, Jo Schlemper, Jose Caballero, Anthony N Price, Joseph V Hajnal, and Daniel Rueckert. Convolutional recurrent neural networks for dynamic mr image reconstruction. *IEEE transactions on medical imaging*, 38(1):280–290, 2018. 3

[29] Joaquin Quiñonero-Candela, Masashi Sugiyama, Neil D Lawrence, and Anton Schwaighofer. *Dataset shift in machine learning*. Mit Press, 2009. 1

[30] Ievgen Redko, Emilie Morvant, Amaury Habrard, Marc Sebban, and Younès Bennani. A survey on domain adaptation theory: learning bounds and theoretical guarantees. *arXiv preprint arXiv:2004.11829*, 2020. 2

[31] Nicola Rieke, Jonny Hancox, et al. The future of digital health with federated learning. *npj Digital Medicine*, 3(1):119, dec 2020. 1

[32] Holger R Roth, Ken Chang, Praveer Singh, Nir Neumark, Wenqi Li, Vikash Gupta, Sharut Gupta, Liangqiong Qu, Alvin Ihsani, Bernardo C Bizzo, et al. Federated learning for breast density classification: A real-world implementation. In *Domain Adaptation and Representation Transfer, and Distributed and Collaborative Learning*, pages 181–191. Springer, 2020. 2

[33] Eduardo Hugo Sanchez, Mathieu Serrurier, and Mathias Ortner. Learning disentangled representations via mutual information estimation. In *European Conference on Computer Vision*, pages 205–221. Springer, 2020. 3

[34] Kihyuk Sohn. Improved deep metric learning with multi-class n-pair loss objective. In *Advances in neural information processing systems*, pages 1857–1865, 2016. 11

[35] Pingfan Song, Lior Weizman, João FC Mota, Yonina C Eldar, and Miguel RD Rodrigues. Coupled dictionary learning for multi-contrast mri reconstruction. *IEEE transactions on medical imaging*, 39(3):621–633, 2019. 2

[36] Anuroop Sriram, Jure Zbontar, Tullie Murrell, C Lawrence Zitnick, Aaron Defazio, and Daniel K Sodickson. Grappnet: Combining parallel imaging with deep learning for multi-coil mri reconstruction. In *Proceedings of the IEEE Conference on Computer Vision and Pattern Recognition*, pages 14315–14322, 2020. 1

[37] Liyan Sun, Zhiwen Fan, Xueyang Fu, Yue Huang, Xinghao Ding, and John Paisley. A deep information sharing network for multi-contrast compressed sensing mri reconstruction. *IEEE Transactions on Image Processing*, 28(12):6141–6153, 2019. 3

[38] Ashish Vaswani, Noam Shazeer, Niki Parmar, Jakob Uszkoreit, Llion Jones, Aidan N Gomez, Łukasz Kaiser, and Illia Polosukhin. Attention is all you need. In *Advances in neural information processing systems*, pages 5998–6008, 2017. 2

[39] Mei Wang and Weihong Deng. Deep visual domain adaptation: A survey. *Neurocomputing*, 312:135–153, 2018. 2

[40] Shanshan Wang, Zhenghang Su, Leslie Ying, Xi Peng, Shun Zhu, Feng Liang, Dagan Feng, and Dong Liang. Accelerating magnetic resonance imaging via deep learning. In *2016 IEEE 13th international symposium on biomedical imaging (ISBI)*, pages 514–517. IEEE, 2016. 2

[41] Haiyan Wu, Yanyun Qu, Shaohui Lin, Jian Zhou, Ruizhi Qiao, Zhizhong Zhang, Yuan Xie, and Lizhuang Ma. Contrastive learning for compact single image dehazing. In *Proceedings of the IEEE/CVF Conference on Computer Vision and Pattern Recognition*, pages 10551–10560, 2021. 4

[42] Qiang Yang, Yang Liu, Tianjian Chen, and Yongxin Tong. Federated Machine Learning: Concept and Applications. *ACM Transactions on Intelligent Systems and Technology*, 10(2):1–19, feb 2019. 1

[43] Qiwei Yuan, Weizhe Hua, Yi Zhou, and Cunxi Yu. Contrastive weight regularization for large minibatch sgd. *arXiv preprint arXiv:2011.08968*, 2020. 4

[44] Jure Zbontar, Florian Knoll, Anuroop Sriram, Tullie Murrell, Zhengnan Huang, Matthew J Muckley, Aaron Defazio, Ruben Stern, Patricia Johnson, Mary Bruno, et al. fastmri: An open dataset and benchmarks for accelerated mri. *arXiv preprint arXiv:1811.08839*, 2018. 5, 6, 7, 12

[45] Bo Zhou and S Kevin Zhou. Dudonet: Learning a dual-domain recurrent network for fast mri reconstruction with deep t1 prior. In *Proceedings of the IEEE/CVF Conference on Computer Vision and Pattern Recognition*, pages 4273–4282, 2020. 1

[46] Bo Zhu, Jeremiah Z Liu, Stephen F Cauley, Bruce R Rosen, and Matthew S Rosen. Image reconstruction by domain-transform manifold learning. *Nature*, 555(7697):487–492, 2018. 1

A. Supplementary Material

A.1. Discussion of Sharing Proportion

Since Scenario 2 has a higher domain-shift, we use this scenario to compare different sharing proportions. Table 5 records the various models with different sharing proportions, where **Ours**₁, **Ours**₂, and **Ours**₃ represent our method with the entire local model shared, with the entire local model except the last layer shared, and with only the first downsampling layer shared. We observe that **Ours**₁ yields the worst results because sharing the entire local model prevents client-specific information from being preserved. From the results of **Ours**₂ and **Ours**₃, we find that the higher the proportion of sharing, the less effective the reconstruction. However, **Ours** achieves the best performance in terms of PSNR and SSIM, suggesting that *designing an effective specificity-preserving FL mechanism for MR image reconstruction is a promising direction*.

A.2. Additional Qualitative Results

We provide additional qualitative improvements regarding the reconstructed images and corresponding error maps under Scenario 1 in Fig. 8. As can be seen from this figure, our method is able to produce the best-quality reconstructed images, and error maps with the least texture. These results are consistent with those of Scenario 2, indicating that *our FedMRI’s reconstructed results are robust under the presence of a domain shift*.

A.3. Computational Cost

To evaluate the speed of our algorithm, we record the training time of all comparison methods on an NVIDIA Tesla V100 GPU under Scenario 2 in Table 4. As can be seen from this table, the training times of our FedMRI[†], LG-FedAvg, and GD-GD are shorter than those of other methods, because they only send a portion of the local model to the server, making them much smaller than the other methods. The training of FedMRI is slower than these partially shared methods because of the introduction of the weighted contrastive regularization term. However, compared with FedAvg [24], FedBN [20], and FedProx [17], our FedMRI has almost no difference in time consumption, but the reconstruction accuracy is definitely improves. Thus, *the computational time of our method is acceptable considering the superior results obtained*. In contrast, the training time of FL-MRCM is twice as long as that of FedMRI[†], mainly due to the repeated adversarial training between the target and source clients.

A.4. Comparison to Other Losses

We further study the effectiveness of different types of losses on our weighted contrastive regularization term, including \mathcal{L}_2 and NT-Xent Loss [2]. Table 6 summarizes the

Methods	Times
FedAvg [24]	80min
FedBN [20]	80min
FL-MRCM [9]	145min
FedProx [17]	83min
LG-FedAvg [21]	75min
GD-GD [1]	76min
FedMRI [†]	73min
FedMRI	84min

Table 4. **Comparison of the average training times per round Scenario 2.** See §A.3 for more details.

reconstruction results of different losses in terms of PSNR and SSIM, where NT-Xent-Contrastive, \mathcal{L}_2 -Contrastive, and \mathcal{L}_1 -Contrastive represent our weighted contrastive regularization term with the NT-Xent, \mathcal{L}_2 , and \mathcal{L}_1 norm, respectively, and *w/o*-Contrastive represents our model without the weighted contrastive regularization term. It is worth noting from this figure that our weighted contrastive regularization using the \mathcal{L}_1 loss achieves the best performance, outperforming the NT-Xent loss by **0.98 dB**, and the \mathcal{L}_2 loss by **0.73 dB**. Compared with *w/o*-Contrastive, we observe that simply using the NT-Xent loss [34] cannot improve the accuracy, and even reduces the reconstruction accuracy of some clients.

Different from most of the current contrastive learning methods, our weighted contrastive regularization explores model weights to replace features and find positive and negative pairs, aiming to correct the direction of local gradient optimization through weighted contrastive regularization. Thus, the local model can be updated while maintaining the performance of the global model. Compared with feature-based contrastive learning, the weighted contrastive regularization method gets rid of the dependence on large batch sizes and yields better reconstruction results (see the ablation study).

Methods	fastMRI [44]		BraTS [25]		SMS [6]		uMR [6]		Average	
	ID uniform 3×		ID Cartesian 5×		2D radial 4×		2D random 6×		PSNR	SSIM
PSNR	SSIM	PSNR	SSIM	PSNR	SSIM	PSNR	SSIM	PSNR	SSIM	
Ours₁	35.26	0.925	29.66	0.869	24.49	0.771	24.25	0.661	28.41	0.806
Ours₂	38.00	0.959	30.07	0.902	37.02	0.970	37.28	0.959	35.59	0.948
Ours₃	36.50	0.935	29.25	0.905	31.63	0.941	31.22	0.931	32.15	0.928
Ours	39.74	0.971	31.18	0.919	38.17	0.970	37.74	0.963	36.71	0.956

Table 5. **Comparison of different sharing proportions** under Scenario 2, where **Ours₁**, **Ours₂**, and **Ours₃** represent our method with the entire local model shared, with the entire local model except the last layer shared, and with only the first downsampling layer shared. See §A.1 for more details.

Methods	fastMRI [44]		BraTS [25]		SMS [6]		uMR [6]		Average	
	ID uniform 3×		ID Cartesian 5×		2D radial 4×		2D random 6×		PSNR	SSIM
PSNR	SSIM	PSNR	SSIM	PSNR	SSIM	PSNR	SSIM	PSNR	SSIM	
w/o-Contrastive	38.42	0.962	30.24	0.915	37.36	0.968	37.44	0.959	35.87	0.951
NT-Xent-Contrastive	39.00	0.965	30.87	0.914	36.37	0.960	36.69	0.951	35.73	0.948
\mathcal{L}_2 -Contrastive	38.98	0.966	30.69	0.913	37.21	0.970	37.02	0.960	35.98	0.952
\mathcal{L}_1 -Contrastive	39.74	0.971	31.18	0.919	38.17	0.970	37.74	0.963	36.71	0.956

Table 6. **Comparison of different loss designs** for the weighted contrastive regularization under Scenario 2, where NT-Xent-Contrastive, \mathcal{L}_2 -Contrastive, and \mathcal{L}_1 -Contrastive represent our weighted contrastive regularization term with the NT-Xent, \mathcal{L}_2 , and \mathcal{L}_1 norm, respectively, and w/o-Contrastive represents our model without the weighted contrastive regularization term. See §A.4 for more details.

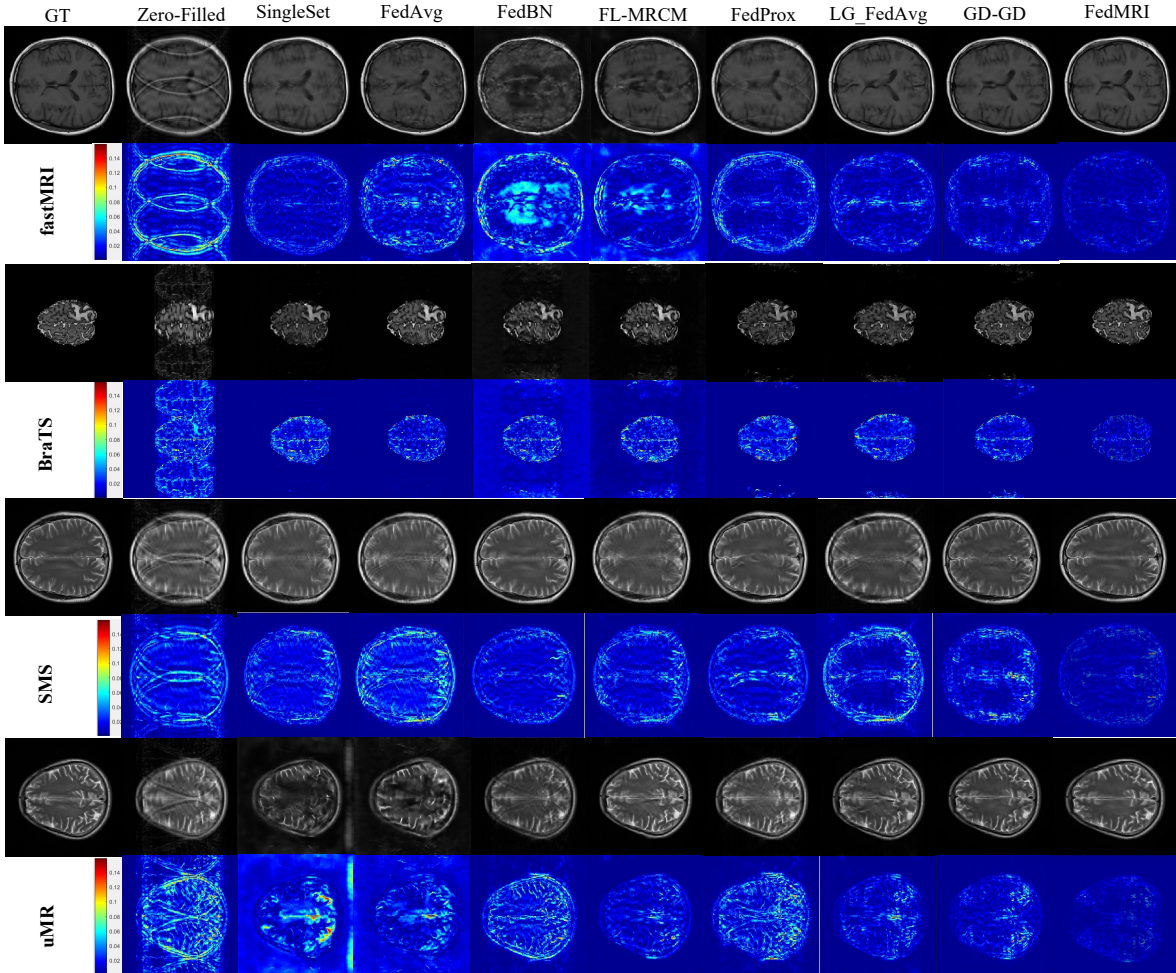


Figure 8. **Qualitative comparison** of different methods in terms of reconstruction quality and error maps under Scenario 1. See §A.2 for more details.